INFLUENCE OF LARGE-SCALE LOW- AND HIGH-SPEED STRUCTURES ON A TURBULENT BOUNDARY LAYER

Jinyul Hwang
Department of Mechanical Engineering
Korea Advanced Institute of Science and Technology (KAIST)
Daejeon 34141, Korea
j.yhwang@kaist.ac.kr

Hyung Jin Sung
Department of Mechanical Engineering
Korea Advanced Institute of Science and Technology (KAIST)
Daejeon 34141, Korea
hjsung@kaist.ac.kr

ABSTRACT

Direct numerical simulation data of a turbulent boundary layer ($Re_\tau \approx 1000$) are used to explore the influences of large-scale structures on the near-wall vortical motions. The streamwise swirling strengths (λ_x) are conditionally sampled in terms of the large-scale streamwise velocity fluctuations (u_l). In the near-wall region, the amplitudes of λ_x diminish under negative u_l rather than under positive u_l. This behaviour is due to the near-wall spanwise motions within the footprints of large-scale structures, which are the congregative and dispersive motions induced by the outer large-scale low-speed and high-speed structures. The intense dispersive motions under the footprint of positive u_l strengthen the small-scale spanwise velocity fluctuations (w_s) close to the wall compared to w_s affected by the congregative motions of negative u_l. The wall-normal velocity components were attenuated or amplified around the modulated vortical motions, which leads to the dependence of λ_x on the large scales. To quantify the contribution of the modulated vortical motions, we use the decomposition method of Yoon *et al*. (2016), which is the relationship between the velocity-vorticity correlations and the skin-friction coefficient (C_f). In the near-wall region, intense values of $\langle -w\omega_y \rangle$, related to change-of-scale effect due to the vortex stretching force, are observed for the positive-u_l event. The skin friction induced by the amplified vortical motions within $u_l^+ > 2$ carries 15% of the total skin friction generated by the change-of-scale effect.

INTRODUCTION

In turbulent boundary layers (TBLs), the outer large-scale structures play a significant role in producing the turbulent kinetic energy and in momentum transfer. These organized motions scale with the outer length scale δ, where δ is the 99% boundary layer thickness. The large-scale structures contribute substantially to the turbulent kinetic energy and the Reynolds shear stress in wall-bounded turbulent flow (Ganapathisubramani et al. 2003; Guala et al. 2006; Balakumar & Adrian 2007; Huthchins & Marusic 2007a; Lee & Sung 2011). In addition, the footprint of the large-scale structures extends to the near-wall region and, thus maintains the large-scale energy in the near-wall region (Hutchins & Marusic 2007a). As a result, a scaling failure in the inner-normalized streamwise turbulence intensity appears (del Álamo & Jiménez 2003; Hutchins & Marusic 2007a), indicating that the outer large-scale structures and the near-wall region are interlinked.

A noteworthy feature of the large-scale structures is their influence on the small scales. Hutchins & Marusic (2007b) showed that the large-scale streamwise velocity fluctuations modulate the amplitudes of the small scales. Mathis et al. (2009) quantified the amplitude modulation (AM) effects of the large scales. Talluru et al. (2014) extended this view to quantify the AM of the small-scale wall-normal and spanwise velocity fluctuations.

Although the aforementioned works characterize the AM effects induced by the large-scale structures, these methods do not differentiate the influences of large-scale low- or high-speed events. The footprint of the high-speed structures is wider than that of the low-speed structures due to the opposing spanwise motions induced by the associated large-scale circulations, which are either congregative or dispersive (Hwang et al. 2016a). The opposing spanwise motions of the large-scale low- and high-speed events are associated with the asymmetric contributions to the Reynolds stresses in the near-wall region (Agostini & Leschziner 2014; Hwang et al. 2016a) and with the attenuation or amplification of the small scales depending on the sign of the large-scale fluctuations observed in the instantaneous fluctuating signals (Hutchins & Marusic 2007b). To account for these observations, therefore, it is necessary to examine the AM effect in terms of the sign of the large scales.

The work of Ganapathisubramani et al. (2012) examined the AM of the small-scale streamwise velocity fluctuations on the sign of the large scales in the TBL. In the near-wall region, the variance of the small scales

conditioned on the negative large scales is lower than that conditioned on the positive large scales, whereas the former exceeds the latter as the wall-normal distance increases. The influence of the large scales on the dissipative scales was reported by Guala et al. (2011). In addition, Ganapathisubramani et al. (2012) found the frequency modulation effect by the large scales below y^+ = 100. Since the vortical structures are responsible for small-scale activities in the near-wall region, the amplitudes of the vortical motions could be influenced by the strength of the large scales. Furthermore, the relationship between the modulated velocity fluctuations and the vortical motions has not yet been elucidated.

The objective of the present study is to elucidate the influence of large-scale low- and high-speed structures on the vortical motions associated with the local skin friction. We analyse the DNS data obtained from a TBL at $Re_\tau \approx$ 1000. The amplitudes of the streamwise vortical structures are conditionally averaged in terms of the strengths of the large-scale streamwise velocity fluctuations. The vortical structures under the influence of large-scale events and their associated velocity fluctuations reveal that the amplification or attenuation of the near-wall vortical motions is closely related to the AM of the velocity fluctuations. Finally, we compute the contribution of the modulated vortical motions to C_f.

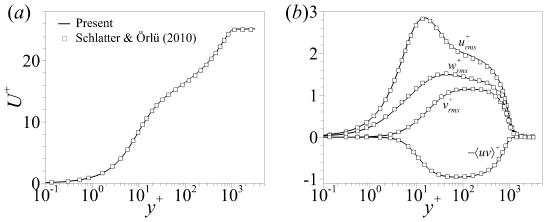

Figure 1 Turbulent statistics at $Re_\tau \approx$ 1000: (*a*) mean streamwise velocity; (*d*) r.m.s of the velocity fluctuations and the Reynolds shear stress.

NUMERICAL DETAILS

The Navier–Stokes equations for incompressible flow are solved using the fractional step method of Kim et al. (2002). In the present work, x, y, and z indicate the streamwise, wall-normal and spanwise directions, respectively. The associated velocity components are u, v and w. Capital letters and an angle bracket are used to represent the ensemble-averaged quantities and lower-case letters indicate the fluctuating components ($u = u - U$). The superscript + denotes quantities normalized by the friction velocity u_τ and viscosity ν. We performed a DNS of a zero pressure gradient boundary layer over a smooth flat plate. The free stream velocity is U_∞, and the inlet boundary layer thickness is δ_0. The no-slip boundary condition is imposed at the wall, and the top boundary condition is $u = U_\infty$, $\partial v / \partial y = 0$ and $w = 0$. The periodic boundary condition is applied in the spanwise direction. At the exit, the convective boundary condition is applied according to $\partial u / \partial t + c(\partial u / \partial x) = 0$, where c is the local bulk velocity. The inflow condition is set as a superposition of the Blasius velocity profile and the isotropic free-stream turbulence generated by the Orr–Sommerfeld and Squire modes in the wall-normal direction and Fourier modes in time and in the spanwise direction (Jacobs & Durbin 2001). The turbulent intensity of the free-stream turbulence is set to 5% and imposed on the Blasius profile up to $y = 2\delta_0$. The domain size (L_x, L_y, L_z) is set to ($2300\delta_0$, $100\delta_0$, $100\delta_0$) and the corresponding grid points are (13313, 541, 769). The spatial resolutions are $\Delta x^+ = 5.49$, $\Delta y^+ = 0.159$–9.56, $\Delta z^+ = 4.13$ at $Re_\tau \approx$ 1000. The boundary layer is spatially developing with the Reynolds number based on the momentum thickness, Re_θ = 109–3240. To validate the present data, the turbulent statistics at $Re_\tau \approx 1000$ are shown in figure 1. The profiles of the present data are in good agreement with the TBL data of Schlatter & Örlü (2010).

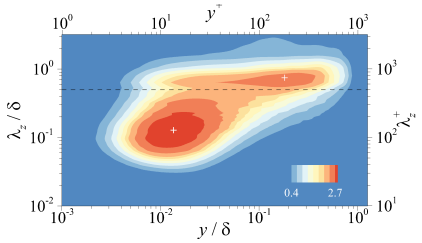

Figure 2 Premultiplied spanwise spectrum of u at $Re_\tau \approx$ 1000. The dashed line represents $\lambda_z/\delta = 0.5$.

Amplitude modulation of the vortical motions

Figure 2 shows the premultiplied spanwise spectrum of u at $Re_\tau \approx$ 1000. Here, λ_z denotes the spanwise wavelength. Two peaks are observed and their positions are marked by the cross symbols. An inner peak appears at (y^+, λ_z^+) = (13, 120), and an outer peak is located at (y/δ, λ_z/δ) = (0.18, 0.75). This outer peak represents a spectral signature of the superstructures, similar to that observed in the premultiplied streamwise spectrum of u (Hutchins & Marusic 2007a). These two energy lobes could be demarcated based on the spanwise wavelength. Hence, the streamwise velocity fluctuations are separated into small (u_s) and large scales (u_l) in the spanwise direction with the cut-off wavelength of $\lambda_z/\delta = 0.5$.

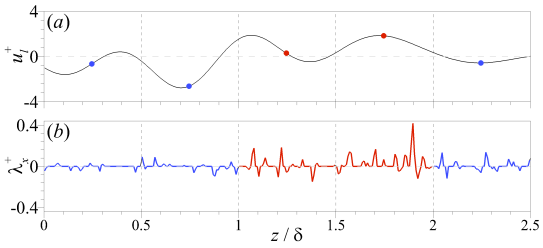

Figure 3 Sample signal of (*a*) large-scale streamwise velocity fluctuations u_l^+ and (*b*) streamwise swirling strengths λ_x^+ at y^+ = 14.5. The circles denote the centre values at each segment.

Next, a conditional sampling analysis is applied to the vortical structures to explore the large-scale influence. The vortical motions are identified by the swirling strength (λ_{ci}), which is the imaginary part of the eigenvalue of the velocity gradient tensor (Zhou et al. 1999). The streamwise swirling strength ($\lambda_{ci,x}$) could be computed using the two-dimensional velocity gradient

tensor. Furthermore, the direction of the swirling motions is demarcated by multiplying the sign of the vorticity fluctuations $\lambda_x = \lambda_{ci,x}\omega_x / |\omega_x|$ (Tomkins & Adrian 2003).

Figure 3 represents a sample signal u_l^+ for λ_x at y^+ = 14.5. Red and blue colours indicate the fluctuating signals with the representative large-scale fluctuations of $u_l > 0$ and $u_l < 0$, respectively. The amplitudes of the swirling strengths are attenuated for $u_l < 0$ and amplified for $u_l > 0$ in the near-wall region. To further explore this behaviour, we compute the r.m.s. of the swirling strength along the wall-normal direction. First, the fluctuating signals are separated into individual segments of length 0.5δ. Then, the r.m.s. of the signals is computed at each segment, and the corresponding value of u_l in a segment is chosen as the centre value of each segment (circles in figure 3a).

$$\langle \lambda_x'(u_l, y) \rangle = \frac{\sum \lambda_x'(y)|_{u_l}}{N[u_l(y)]} \qquad (1)$$

where $N[u_l(y)]$ is the number of occurrences of u_l.

The conditionally averaged swirling strengths (1) represent the amplitudes of the vortical motions conditioned on the strength of u_l along the wall-normal direction. Figure 4(a) demonstrates the conditioned r.m.s. of the swirling strengths $\langle \lambda_x' \rangle$. In the near-wall region, intense regions appears for the positive-u_l event, and their magnitudes decrease with decreasing u_l, indicating that the amplitude of the vortical structures depends on the strength of the large scales. As y increases $\langle \lambda_x' \rangle$ decreases regardless of the strength of u_l, but the rate of decrease depends on u_l. Figure 4(b) shows the profiles of $\langle \lambda_x' \rangle$ at $u_l^+ = -2$, 0 and 2. The intensity of the swirling strengths for $u_l^+ = 2$ is greater than that for $u_l^+ = -2$ in the near-wall region. Above $y^+ \approx 100$, the swirling strengths under the negative-u_l event exceed those under the positive-u_l event. The AM of the swirling strength is similar to that observed in the AM of the velocity fluctuations, indicating that the large-scale influence on the small-scale velocity fields is related to the AM of the vortical structures. In the subsequent section, we will explore the conditionally averaged velocity fields around the modulated swirling motions to investigate how the vortical motions are attenuated or amplified by focusing on the relation between the modulated swirling strengths and their associated velocity fields.

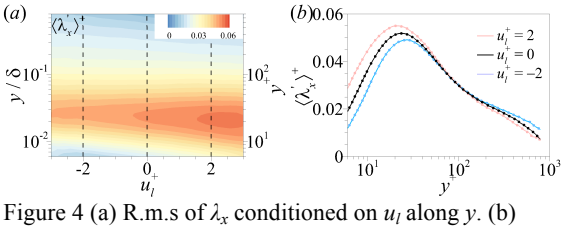

Figure 4 (a) R.m.s of λ_x conditioned on u_l along y. (b) Profiles of $\langle \lambda_x' \rangle$ for $u_l^+ = -2$, 0 and 2.

CONDITIONALLY AVEARGED ANALYSIS

We first examine the flow field around the near-wall u_l. The conditionally averaged velocities for the negative- and positive-u_l events are defined as

$$\langle \boldsymbol{u}|^{nl}(r_x, y, r_z) \rangle = \langle \boldsymbol{u}(x + r_x, y, z + r_z) | u_l^+(x, y_{ref}, z) < -2 \rangle, \qquad (2)$$

$$\langle \boldsymbol{u}|^{pl}(r_x, y, r_z) \rangle = \langle \boldsymbol{u}(x + r_x, y, z + r_z) | u_l^+(x, y_{ref}, z) > +2 \rangle. \qquad (3)$$

Here, the superscript *nl* and *pl* denotes large-scale low- and high-speed conditions, respectively. The reference wall-normal position is y^+ = 14.5. Figure 5(a,b) represents isosurfaces of $\langle u|^{nl} \rangle$ and $\langle u|^{pl} \rangle$. Although the reference wall-normal position is located at y_{ref}^+ = 14.5, the conditional structures extended beyond the buffer layer (their height was approximately 0.4δ) as well as have their streamwise length over 2δ. On the contrary, the conditional structures for the weak strength of u_l ($|u_l^+(x, y_{ref}, z)| < 0.2$) are enclosed within the buffer region (not shown here). Therefore, the condition $|u_l^+(x, y_{ref}, z)| > 2$ can be considered as the footprints of the outer large-scale structures. In figures 6 and 7, the near-wall vortical structures under the footprints of the large-scale structures are investigated based on this condition.

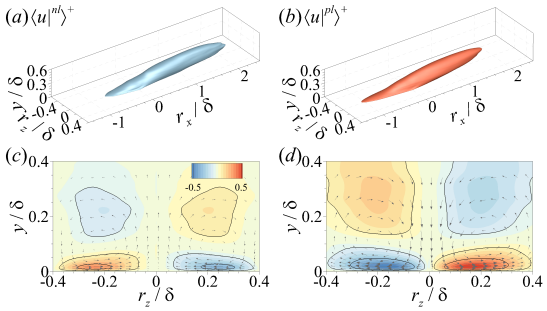

Figure 5 (a,b) Conditional structures associated with the footprints of large-scale low- and high-speed structures; $\langle u|^{nl} \rangle^+ = -1.0$ (blue) and $\langle u|^{pl} \rangle^+ = +1.0$ (red). Contours of spanwise velocity fluctuations (c) $\langle w|^{nl} \rangle^+$ and (d) $\langle w|^{pl} \rangle^+$ in the cross-stream plane (r_x/δ = 0). Inserted vector represents the in-plane velocity components.

Figure 5(c,d) illustrates the cross-stream plane of the conditionally averaged field at $r_x/\delta = 0$. Both the negative- and positive-u_l events show a pair of roll motions whose centres are located at $y/\delta = 0.1$; for the weak u_l^+ condition, the smaller circulations are observed and their centres are at $y^+ = 30$. The flow fields associated with each structures have remarkably distinct features. For the negative u_l (figure 5c), the ejection event occurs whereas the sweep event is observed in the conditional structure of the positive u_l (figure 5d). As a result of the opposite wall-normal motions (i.e. $v > 0$ and $v < 0$ for ejections and sweeps), each conditional structures induce opposite spanwise near-wall motions. In addition, the maximum $\langle w|^{pl} \rangle^+$ is 0.63 (1.2 times greater than the maximum $\langle w|^{nl} \rangle^+$, indicating that the strength of the dispersive motions induced by $u_l > 0$ are intense compared to the congregative motion. The congregative motion related to the outer ejections is reduced, because the spanwise motion under the large-scale circulation on both sides of the negative structure decreases as the flows come close to each other. On the other hand, the sweep of high-

momentum fluid toward the wall leads to the enhancement of the spanwise momentum. Therefore, the different magnitudes of the spanwise motion arise from the nature of low- and high-speed structures. The influence of large-scale structures on the near-wall vortical structures is examined by focusing on the congregative and dispersive motions induced by $u_l < 0$ and $u_l > 0$, respectively.

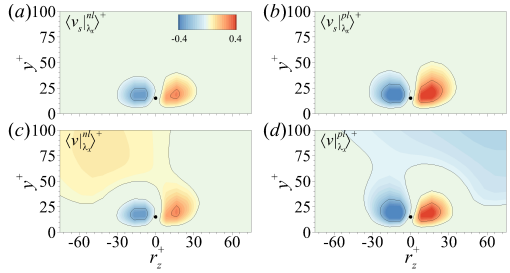

Figure 6 (*a*,*b*) $\langle v_s|^{nl}_{\lambda_x}\rangle$ and $\langle v_s|^{pl}_{\lambda_x}\rangle$ in the *y*–*z* plane ($r_x^+ = 0$). (*c*,*d*) $\langle v|^{nl}_{\lambda_x}\rangle$ and $\langle v|^{pl}_{\lambda_x}\rangle$ in the *y*–*z* plane ($r_x^+ = 0$).

The differences in λ_x obtained under the negative and positive u_l are further examined by educing the flow field around the modulated λ_x, which provides a connection to the amplified or attenuated small-scale velocity fluctuations ($\boldsymbol{u}_s$). The conditionally averaged $\boldsymbol{u}_s$ associated with the modulated λ_x under the footprints of the negative and positive u_l are defined as

$$\langle \boldsymbol{u}_s|^{nl}_{\lambda_x}(r_x, y, r_z)\rangle = \langle \boldsymbol{u}_s(x + r_x, y, z + r_z)|E_1(x, y_{ref}, z)\rangle, \quad (4)$$

$$\langle \boldsymbol{u}_s|^{nl}_{\lambda_x}(r_x, y, r_z)\rangle = \langle \boldsymbol{u}_s(x + r_x, y, z + r_z)|E_2(x, y_{ref}, z)\rangle, \quad (5)$$

where $E_1 = \{\lambda_x(x, y_{ref}, z) > 0 \;\&\; u_l^+(x, y_{ref}, z) < -2\}$ and $E_2 = \{\lambda_x(x, y_{ref}, z) > 0 \;\&\; u_l^+(x, y_{ref}, z) > 2\}$. Figure 6(*a*,*b*) and 7(*a*,*b*) shows the educed cross-stream components of the small scales ($\langle v_s|_{\lambda_x}\rangle$ and $\langle w_s|_{\lambda_x}\rangle$), which contribute to the streamwise swirling motions, in the *y*–*z* plane ($r_x^+ = 0$). The flow fields of both the negative- and positive-u_l events indicate the presence of a counter-clockwise swirling motion around the reference position. However, the magnitudes of both $\langle v_s|_{\lambda_x}\rangle$ and $\langle w_s|_{\lambda_x}\rangle$ depend on the large-scale event. For the small-scale wall-normal components (figure 6*a* and *b*), the positive and negative regions are intense under the positive-u_l event compared to the negative-u_l event. For the small-scale spanwise components (figure 7*a* and *b*), the negative- and positive-w_s region is located above and below the centre of the vortex. In particular, the positive-w_s region is noticeably strengthened under the positive-u_l event, whereas the negative-w_s region have comparable magnitudes under the negative- and positive-u_l event (compare figure 7a with b); the minimum value is −0.6 for both events, while the maximum values $\langle w_s|^{pl}_{\lambda_x}\rangle^+$ of and $\langle w_s|^{nl}_{\lambda_x}\rangle^+$ are 0.9 and 0.6, respectively.

A noteworthy feature of figure 7(*a*,*b*) is that only the positive-w_s region ($y < y_{ref}$) is strengthened under the positive-u_l event. In contrast to the modulation of v_s, this behaviour represents that the large-scale high-speed structure enhance the amplitude of w_s below the centre of the vortical motions. This phenomenon is further investigated by conditionally averaging the total velocity fluctuations ($\boldsymbol{u}$). The educed cross-stream components of the total fluctuations ($\langle v|_{\lambda_x}\rangle$ and $\langle w|_{\lambda_x}\rangle$) are illustrated in figure 6(*c*,*d*) and 7(*c*,*d*). The cross-stream components clearly differ from the educed small scales (compare figures 6*a*,*b* and 7*a*,*b* respectively with 6*c*,*d* and 7*c*,*d*) due to the presence of large scales. Note that the educed total velocity fluctuations for the weak u_l represent an absence of large-scale circulations, revealing that the large-scale features shown here are important for explaining the asymmetric influence of the negative- and positive-u_l event on the vortical motions.

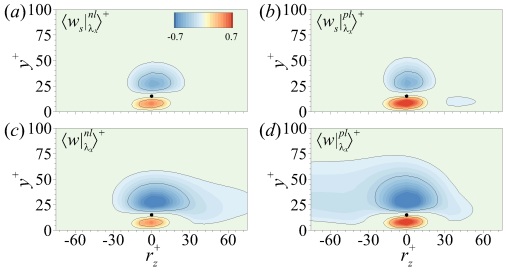

Figure 7 (*a*,*b*) $\langle w_s|^{nl}_{\lambda_x}\rangle$ and $\langle w_s|^{pl}_{\lambda_x}\rangle$ in the *y*–*z* plane ($r_x^+ = 0$). (*c*,*d*) $\langle w|^{nl}_{\lambda_x}\rangle$ and $\langle w|^{pl}_{\lambda_x}\rangle$ in the *y*–*z* plane ($r_x^+ = 0$).

In figure 6(*c*,*d*), the wall-normal component includes wide regions of positive and negative *v* beyond the buffer region, associated with the outer ejection and sweep events induced by large-scale structures. Likewise, congregative and dispersive motions, represented by the intense negative-*w* regions above $y > y_{ref}$, are observed in figure 7(*c*,*d*). The magnitudes of the positive *w* ($y < y_{ref}$) in figure 7(*c*,*d*) are similar to the positive w_s in figure 7(*a*,*b*); the maximum values of $\langle w|^{pl}_{\lambda_x}\rangle^+$ and $\langle w|^{nl}_{\lambda_x}\rangle^+$ are 0.9 and 0.6, respectively, analogous to those of $\langle w_s|^{pl}_{\lambda_x}\rangle^+$ and $\langle w_s|^{nl}_{\lambda_x}\rangle^+$. In other words, the large scales are not superimposed on the spanwise velocity fluctuations below the centre of the modulated vortical structures, whereas the large-scale spanwise motions appear above the centre of the modulated vortical structures. There are negative-*w* regions of $\langle w|^{pl}_{\lambda_x}\rangle^+$ with a greater magnitude compared to that of $\langle w|^{nl}_{\lambda_x}\rangle^+$, reminiscent of the strong dispersive motions within the footprint of positive u_l (c.f. figure 5*d*). The strong dispersive motions induced by positive-u_l structures, strengthen the opposite spanwise motion (positive-w_s region in figure 7*b*), whereas the small-scale spanwise component is relatively weakened under the negative-u_l event.

LARGE-SCALE INFLUENCE ON THE SKIN-FRICTION COEFFICIENT

We analyze the contribution of the modulated vortical motions to the skin friction since the amplification and attenuation of λ_x, and also their associated velocity fields

can give an influence on local skin-friction coefficient (C_f). In order to quantify the contribution of the modulated vortical motions on C_f, we use a new decomposition method for C_f suggested by Yoon *et al*. (2016). Using this method, C_f could be decomposed into five parts,

$$C_f = \underbrace{\int_0^1 2\left(1-\frac{y}{\delta}\right)\frac{\langle v\omega_z\rangle}{U_\infty^2/\delta}\mathrm{d}\left(\frac{y}{\delta}\right)}_{C_{f1}} + \underbrace{\int_0^1 2\left(1-\frac{y}{\delta}\right)\frac{\langle -w\omega_y\rangle}{U_\infty^2/\delta}\mathrm{d}\left(\frac{y}{\delta}\right)}_{C_{f2}} + \underbrace{\frac{\nu\delta}{U_\infty^2}\frac{\partial\Omega_z}{\partial y}\bigg|_{y=0}}_{C_{f3}} + \underbrace{\frac{\nu}{U_\infty^2}\int_0^1 -2\Omega_z\mathrm{d}\left(\frac{y}{\delta}\right)}_{C_{f4}} + \underbrace{\int_0^1\left(1-\frac{y}{\delta}\right)^2\frac{\langle I_x\rangle}{U_\infty^2}\frac{\delta^2}{}\mathrm{d}\left(\frac{y}{\delta}\right)}_{C_{f5}}, \tag{6}$$

$$\langle I_x\rangle = \frac{\partial}{\partial x}\left(U\Omega_z + \langle u\omega_z\rangle - \langle w\omega_x\rangle\right) + \frac{\partial}{\partial y}\left(V\Omega_z\right) - \nu\frac{\partial^2\Omega_z}{\partial x^2}. \tag{7}$$

The first and second terms (C_{f1} and C_{f2}) indicate the skin friction induced by the velocity-vorticity correlations $\langle v\omega_z\rangle$ and $\langle w\omega_y\rangle$. The third and fourth terms (C_{f3} and C_{f4}) indicate the contributions of the molecular diffusion at the wall and the molecular transfer due to the mean vorticity, respectively. The last term (C_{f5}) is the contribution of a spatial development term $\langle I_x\rangle$ (7). In the present study, we focus on the second term (C_{f2}) because the term $\langle -w\omega_y\rangle$ is associated with the change-of-scale effect related to the vortex-stretching force (Tennekes & Lumley 1972). In addition, $\langle -w\omega_y\rangle$ is closely related to the AM (change of length scale) of the small scales by the large-scale motions (Chin *et al*. 2014; Hwang *et al*. 2016*b*).

We first compute $\langle -w\omega_y\rangle$ conditioned on the strength of u_l similar to (1). Figure 8(*a*) represents the contour of $\langle -w\omega_y(u_l,y)\rangle^+$. In the near-wall region, intense regions appear for the positive u_l and $\langle -w\omega_y(u_l,y)\rangle^+$ decreases with decreasing u_l. Figure 19(*b*) plots the profiles of $\langle -w\omega_y(u_l,y)\rangle^+$ for $u_l^+ = -2$, 0 and 2. The profiles reach a distinct peak at $y^+ \approx 12$ and decay rapidly as y increases. The profile of $\langle -w\omega_y(u_l,y)\rangle^+$ for $u_l^+ = -2$ crosses zero at $y^+ \approx 100$, indicating that the vortex stretching in this region negatively contributes to C_{f2}. For $u_l^+ = 2$, by contrast, the profile of $\langle -w\omega_y\rangle$ is positive and reaches a higher magnitude along the wall-normal direction; thus, the vortex stretching under the influence of positive u_l enhances C_f.

Next, the frictional drag induced by the modulated $\langle -w\omega_y\rangle$ is examined by obtaining the second term in (6) as a function of u_l,

$$\langle C_{f2}(u_l)\rangle = \int_0^1 2\left(1-\frac{y}{\delta}\right)\frac{\langle -w\omega_y(u_l,y)\rangle}{U_\infty^2/\delta}\mathrm{d}\left(\frac{y}{\delta}\right). \tag{9}$$

In figure 8(*c*), the skin friction induced by the vortex stretching effect varies with the strength of u_l, indicating that the modulation of vortical motions is directly attributed to the dependence of the local skin friction on the large-scale structures. Here, the horizontal line indicates C_{f2} in (6). The value of $\langle C_{f2}(u_l)\rangle$ for the positive u_l exceeds the value of C_{f2}, whereas this trend is reversed for the negative u_l. The amplified vortical motions within the footprint of positive u_l induces the high skin friction. Conversely, the vortical motions, which are attenuated within the footprint of the negative u_l, contribute to the low skin friction.

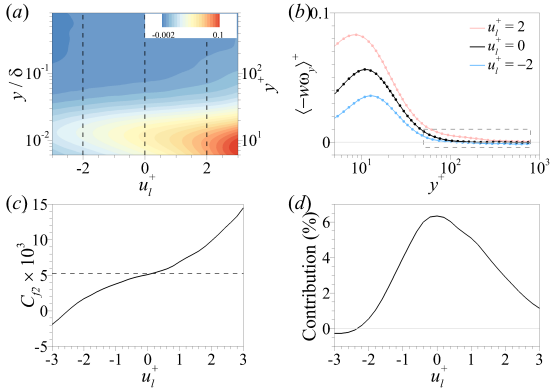

Figure 8 (*a*) Conditionally averaged velocity-vorticity correaltion $\langle -w\omega_y(u_l,y)\rangle^+$. (*b*) Profiles of $\langle -w\omega_y(u_l,y)\rangle^+$ for $u_l^+ = -2$, 0 and 2. (*c*) Skin friction induced by $\langle -w\omega_y(u_l,y)\rangle$, $\langle C_{f2}(u_l)\rangle$. (*d*) Contribution of $\langle C_{f2}(u_l)\rangle$ to C_{f2}, $C_{f2}^{con}(u_l)$.

Next, we consider the contribution of $\langle C_{f2}(u_l)\rangle$ to C_{f2}. The contribution of $\langle C_{f2}(u_l)\rangle$ (C_{f2}^{con}) could be computed according to

$$C_{f2}^{con}(u_l) = \frac{1}{C_{f2}}\int_0^1 2\left(1-\frac{y}{\delta}\right)\frac{\langle -w\omega_y(u_l,y)\rangle}{U_\infty^2/\delta}C(u_l,y)\mathrm{d}\left(\frac{y}{\delta}\right), \tag{10}$$

$$C(u_l,y) = \frac{N[u_l(y)]}{\sum N[u_l(y)]}. \tag{11}$$

As shown in figure 8(*d*), the plot of $C_{f2}^{con}(u_l)$ is not symmetric with respect to $u_l^+ = 0$. A peak appears at $u_l^+ = 0$ due to the dominance of the weak-u_l event. The contribution of $u_l < 0$ is quite small compared to that of $u_l > 0$. A negative contribution is observed in the range $u_l^+ < -2.3$ because $\langle -w\omega_y\rangle < 0$ in the outer region become dominant compared to $\langle -w\omega_y\rangle > 0$ in the near-wall region. As a result, the cumulative contribution of $u_l^+ < -2$ is nearly zero, whereas the vortex stretching within $u_l^+ > 2$ is responsible for 15% of the contribution to C_{f2}; the cumulative contribution of $u_l^+ < -1$ and $u_l^+ > 1$ is 11% and 36%, respectively. The dispersive motion of the positive u_l enhances the small-scale velocity fluctuations as well as the streamwise vortical motions, which are related to the intense vortex stretching effect. As a result, the amplification effect of the positive-u_l structure dominantly contributes to the skin friction, in contrast to the negative-u_l structures.

SUMMARY AND CONCLUSIONS

We investigate the influence of large-scale low- and high-speed structures on the vortical motions. The large-scale streamwise velocity fluctuations (u_l) are extracted by employing a spanwise wavelength filter ($\lambda_z/\delta > 0.5$). The r.m.s. of the streamwise swirling strength (λ_x) is conditionally sampled as a function of the strength of u_l. The swirling strength is attenuated or amplified under the negative- or positive-u_l events in the near-wall region,

respectively. The asymmetric influence of the large scales on the near-wall region is due to the associated spanwise motions within the footprints of u_l, i.e., the congregative and dispersive motions induced by the outer large-scale low- ($u_l < 0$) and high-speed structures, respectively. The dispersive motions are more intense than the congregative motions. Conditionally averaged velocity fields associated with the vortical structures under the footprints show that the modulated swirling motions lie within the congregative and dispersive motions. The intense dispersive motions under the positive-u_l event strengthen the small-scale spanwise velocity fluctuations (w_s) close to the wall compared to w_s associated with the attenuated vortical motions under the congregative motion. In addition, the wall-normal velocity components around the near-wall swirling motions are attenuated or amplified, which is attributed to the modulation of λ_x on the large scales. We quantify the contribution of the modulated vortical motions to the skin friction by employing the decomposition method of Yoon et al. (2016). The velocity-vorticity correlation $\langle -w\omega_y \rangle$ is the dominant contribution to the total skin friction, and this term is related to the change of size of eddies by the large-sale motions. In the near-wall region, intense values of $\langle -w\omega_y \rangle$ appear for the positive u_l and decrease with decreasing u_l in connection with the amplification of w_s by the strong dispersive motions. The skin friction induced by the amplified vortical motions within $u_l^+ > 2$ carries 15% of the total C_{f2}. These results imply that manipulating the positive-u_l structures, which amplify the near-wall motions through dispersive motions, may provide a means for controlling the turbulence and that computing the contribution of $\langle -w\omega_y \rangle$ to the skin friction offers a reliable measure for evaluating new control strategies in terms of the amplitude modulation effect of outer large-scale structures.

ACKNOWLEDGEMENTS

This work was supported by the Creative Research Initiatives (No. 2017-0013369) program of the National Research Foundation of Korea (MSIP) and was partially supported by KISTI under the Strategic Supercomputing Support Program.

REFERENCES

Agostini, L. & Leschziner, M. A. 2014 On the influence of outer large-scale structures on near-wall turbulence in channel flow. *Phys. Fluids* 26 (7), 075107.

del Álamo, J. C. & Jiménez, J. 2003 Spectra of the very large anisotropic scales in turbulent channels. *Phys. Fluids* 15 (6), L41.

Balakumar, B. J. & Adrian, R. J. 2007 Large-and very-large-scale motions in channel and boundary-layer flows. *Phil.Trans. R. Soc. A* 365 (1852), 665–681.

Chin, C., Philip, J., Klewicki, J., Ooi, A. & Marusic, I. 2014 Reynolds-number-dependent turbulent inertia and onset of log region in pipe flows. *J. Fluid Mech*. 757, 747–769.

Ganapathisubramani, B., Hutchins, N., Monty, J. P., Chung, D. & Marusic, I. 2012 Amplitude and frequency modulation in wall turbulence *J. Fluid Mech*. 712, 61–91.

Ganapathisubramani, B., Longmire, E. K. & Marusic, I. 2003 Characteristics of vortex packets in turbulent boundary layers *J. Fluid Mech.* 478, 35–46.

Guala, M., Hommema, S. E. & Adrian, R. J. 2006 Large-scale and very-large-scale motions in turbulent pipe flow. *J. Fluid Mech*. 554, 521–542.

Guala, M., Metzger, M. & McKeon, B. J. 2011 Interactions within the turbulent boundary layer at high Reynolds number. *J. Fluid Mech*. 666, 573–604.

Hutchins, N. & Marusic, I. 2007a Evidence of very long meandering features in the logarithmic region of turbulent boundary layers. *J. Fluid Mech*. 579, 1–28.

Hutchins, N. & Marusic, I. 2007b Large-scale influences in near-wall turbulence. *Phil. Trans. R. Soc. A* 365 (1852), 647–664.

Hwang, J., Lee, J., Sung, H. J. & Zaki, T. A. 2016a Inner-outer interactions of large-scale structures in turbulent channel flow. *J. Fluid Mech*. 790, 128–157.

Hwang, J., Lee, J., & Sung, H. J. 2016b Influence of large-scale accelerating motions on turbulent pipe and channel flows. *J. Fluid Mech*. 804, 420–441.

Jacobs, R. G. & Durbin, P. A. 2001 Simulations of bypass transition. *J. Fluid Mech*. 428, 185–212.

Lee, J. H. & Sung, H. J. 2011, Very-large-scale motions in a turbulent boundary layer *J. Fluid Mech.* 673, 80–120.

Mathis, R., Hutchins, N. & Marusic, I. 2009 Large-scale amplitude modulation of the small- scale structures in turbulent boundary layers. *J. Fluid Mech*. 628, 311–337.

Schlatter, P. & Örlü R. 2010, Assessment of direct numerical simulation data of turbulent boundary layers. *J. Fluid Mech*. 659, 116–126.

Talluru, K. M., Baidya, R., Hutchins, N. & Marusic, I. 2014 Amplitude modulation of all three velocity components in turbulent boundary layers. *J. Fluid Mech*. 746, R1.

Tennekes, H. & Lumley, J. L. 1972 A First Course in Turbulence. MIT Press.

Tomkins, C. D., & Adrian, R. J. 2003 Spanwise structure and scale growth in turbulent boundary layers. *J. Fluid Mech*. 490, 37–74.

Yoon, M., Ahn, J., Hwang, J., & Sung, H. J. 2016, Contribution of velocity-vorticity correlations to the frictional drag in wall-bounded turbulent flows *Phys. Fluids* 28 (8), 081702.

Zhou, J., Adrian, R. J., Balachandar, S. & Kendall, T. M. 1999 Mechanisms for generating coherent packets of hairpin vortices in channel flow. *J. Fluid Mech*. 387, 353–396